

Nearshore Tsunami Inundation Model Validation: Toward Sediment Transport Applications

ALEX APOTSOS,¹ MARK BUCKLEY,² GUY GELFENBAUM,¹ BRUCE JAFFE,² and DEEPAK VATVANI³

Abstract—Model predictions from a numerical model, Delft3D, based on the nonlinear shallow water equations are compared with analytical results and laboratory observations from seven tsunami-like benchmark experiments, and with field observations from the 26 December 2004 Indian Ocean tsunami. The model accurately predicts the magnitude and timing of the measured water levels and flow velocities, as well as the magnitude of the maximum inundation distance and run-up, for both breaking and non-breaking waves. The shock-capturing numerical scheme employed describes well the total decrease in wave height due to breaking, but does not reproduce the observed shoaling near the break point. The maximum water levels observed onshore near Kuala Meurisi, Sumatra, following the 26 December 2004 tsunami are well predicted given the uncertainty in the model setup. The good agreement between the model predictions and the analytical results and observations demonstrates that the numerical solution and wetting and drying methods employed are appropriate for modeling tsunami inundation for breaking and non-breaking long waves. Extension of the model to include sediment transport may be appropriate for long, non-breaking tsunami waves. Using available sediment transport formulations, the sediment deposit thickness at Kuala Meurisi is predicted generally within a factor of 2.

Key words: Tsunami, inundation, run-up, benchmark validation, numerical modeling.

1. Introduction

The 26 December 2004 tsunami in the Indian Ocean killed over 237,000 people and left more than a million homeless (U.S. Agency for International Development (USAID), 2005). With a large segment of the world's population living along coasts, major

tsunamis have the potential to produce similar disasters in the future. In order to develop appropriate coastal management strategies that properly plan for and mitigate losses owing to tsunamis, researchers have generally focused on two approaches. The first involves coupling early detection systems with numerical models that predict, in real-time, areas most likely to be impacted by a tsunami (e.g., WEI *et al.*, 2008; TANG *et al.*, 2009). The second involves improving local tsunami hazard assessments through a better understanding of the recurrence interval and magnitude of historic and pre-historic tsunamis (e.g., GONZÁLEZ *et al.*, 2009). Both of these approaches require a detailed understanding of the physical processes that occur during a tsunami, particularly the dynamics of nearshore propagation and inundation. The second approach also requires a detailed understanding of how tsunamis transport and deposit sediment. Here, we validate a hydrodynamic model and demonstrate that extending it to include sediment transport produces reasonable results that compare well with field observations.

Unfortunately, the infrequent and unpredictable nature of tsunamis makes it difficult to collect detailed measurements of the physical processes that occur. Therefore, to better understand tsunami processes, analytical, laboratory, and numerical experiments have been conducted. While much of the early work focused on analytical solutions to simplified problems (e.g., CARRIER and GREENSPAN, 1958; TADEPALLI and SYNOLAKIS, 1994, 1996; CARRIER *et al.*, 2003; KÁNOGLU, 2004) and laboratory experiments employing solitary waves (e.g., SYNOLAKIS, 1987; BRIGGS *et al.*, 1995, 1996), recent increases in processing power have greatly improved the utility of numerical models. These models can now be used to predict the propagation and inundation paths of tsunamis in almost real-time (e.g., TITOV *et al.*, 2005; WEI *et al.*, 2008; TANG

¹ Pacific Coastal and Marine Science Center, USGS, 345 Middlefield Rd, MS 999, Menlo Park, CA, USA. E-mail: aapotsos@usgs.gov

² Pacific Coastal and Marine Science Center, USGS, 400 Natural Bridges Drive, Santa Cruz, CA, USA.

³ Deltares, Delft, The Netherlands.

et al., 2009). The use of numerical models in this operational sense has allowed for the rapid determination of which communities are at risk once a tsunami has been detected, and has helped coastal planners and emergency responders act accordingly.

Numerical models can also play a role in improving tsunami hazard assessments, which are often constrained by our limited knowledge of the historic and pre-historic tsunami record. In order to estimate the probability that a major tsunami will strike a specific location, information is needed concerning tsunamis that occurred hundreds or thousands of years ago. Typically the only evidence that remains from these paleo-tsunamis is preserved in the geologic record as a sedimentary layer (e.g., ATWATER, 1987). Dating the soil layers surrounding these deposits can help identify approximately when the tsunami occurred, and thus increase our understanding of the recurrence interval of major tsunamis.

To improve hazard assessments, knowledge of the hydrodynamic characteristics of the tsunami is also necessary. Therefore, significant efforts have been made to use the information (e.g., sediment size, deposit thickness, grading) preserved in tsunami sediment deposits to estimate the wave height, flow depth, and velocity of paleo-tsunamis (e.g., JAFFE and GELFENBAUM, 2007; SMITH *et al.*, 2007; NANAYAMA *et al.*, 2007). These efforts, as well as efforts to understand the scouring that occurs around obstacles during tsunamis, would benefit from a better understanding of how sediment is transported and deposited by a tsunami. Numerical models that accurately predict the hydrodynamic processes of a tsunami could be coupled with sediment suspension and transport formulations and used to determine which processes dominate tsunami sediment transport and what information concerning the source mechanism and hydrodynamic characteristics of the tsunami is retained in tsunami sediment deposits.

Before a hydrodynamic model can be coupled with sediment transport formulations, it must be shown to depict accurately the hydrodynamic processes of a tsunami. Recent deployment of DART (Deep-Ocean Assessing and Reporting of Tsunamis) underwater buoys (e.g., GONZALEZ *et al.*, 2005) and the use of satellite imagery (e.g., ARCAS and TITOV, 2006) have improved model validation in the deep

ocean. However, while analyses of video recordings have provided a few estimates of onshore tsunami flow velocities (FRITZ *et al.*, 2006), detailed observations in the nearshore and on land, where sediment transport is important, are limited. Model evaluation for these regions is therefore still primarily done using analytical and laboratory experiments.

Over the past two decades attempts have been made to standardize the process of model evaluation to ensure the accuracy of model predictions. To this end, a set of benchmarks was developed during the International Workshops on Long-Wave Run-up (e.g., YEH *et al.*, 1996; LIU *et al.*, 2008), and a procedure for model verification was outlined (SYNOLAKIS *et al.*, 2007, 2008). Following the establishment of these initial benchmarks, several other useful laboratory experiments have been conducted and the data made available (see BALDOCK *et al.*, 2008; SWILGER, 2009). However, while detailed comparisons with laboratory observations remain a widely used method to test and validate numerical tsunami models, especially in the nearshore, the use of laboratory observations is not without problems (see MADSEN *et al.*, 2008 and Sect. 4.1 in this paper), and offers only qualified model validation.

Here the results from a hydrodynamic numerical model, Delft3D, are compared with seven tsunami-like benchmarks, and with maximum water level observations measured near Kuala Meurisi, Sumatra, following the 26 December 2004 Indian Ocean tsunami (JAFFE *et al.*, 2006). The benchmarks include: (1) the analytical solution of run-up on a plane beach (CARRIER *et al.*, 2003), and laboratory experiments using (2) a piece-wise linear bathymetry (BALDOCK *et al.*, 2008), (3) an alongshore non-uniform beach (SWILGER, 2009), (4) a circular island amid a constant depth basin (BRIGGS *et al.*, 1995), (5) an alongshore non-uniform beach with a circular island (http://isec.nacse.org/workshop/isec_workshop_2009), (6) a complex three-dimensional beach (Monai Valley, Japan as described in SYNOLAKIS *et al.* (2008), and (7) a piece-wise linear bathymetry ending in a vertical wall (BRIGGS *et al.*, 1996).

Our primary goal in this paper is to demonstrate, to the extent possible, that Delft3D is appropriate for modeling the hydrodynamic processes that occur during the nearshore propagation and inundation of a

tsunami, and to examine the appropriateness of including sediment transport in the model. Verification that Delft3D accurately predicts the hydrodynamic processes that occur during inundation is advantageous because the model includes a sophisticated sediment transport model that has been extensively validated in a wide variety of coastal settings (LESSER *et al.*, 2004; VAN RIJN *et al.*, 2007). This transport model allows sediment particles of varying sizes to be transported in bed or suspended load, the vertical and horizontal structures of any onshore sediment deposits to be determined, and the morphological change associated with sediment transport to be predicted. These features position the model well to be a powerful tool for improving our understanding of how tsunamis transport and deposit sediment.

The numerical model is described in Sect. 2 and the model-data comparisons are outlined in the subsections of Sect. 3. The relevance of the benchmarks to real tsunamis, a preliminary application of the model to sediment transport, and the applicability of the model are discussed in Sect. 4. Conclusions are given in Sect. 5.

2. Model

Delft3D is a three-dimensional numerical model that can simulate coupled hydrodynamic/sediment transport/morphological change processes. This study examines primarily the hydrodynamic model, which solves the nonlinear shallow water equations (NLSWEs) on a three-dimensional staggered grid using a finite difference scheme (STELLING and VAN KESTER, 1994) and the Alternating Direction Implicit time-integration method (STELLING and LEENDERTSE, 1991). The Delft3D model can be run as either a depth-averaged or vertically layered (i.e., three-dimensional) model. In the horizontal, a curvilinear or spherical staggered grid is used. In the vertical (in the case of three-dimensional simulations) sigma layers, which are a fixed percentage of the water depth, or fixed elevation layers are used. When the model is run in three dimensions, the vertical velocity within each grid cell is calculated from the continuity equation due to the hydrostatic assumption and

incompressibility of the flow. The extension of the model to three dimensions is important for many applications where resolution of the bottom boundary layer or vertical stratification within the flow is important (i.e., see Sect. 4.2).

Numerous methods have been developed to solve the NLSWEs. The numeric solver used here is based on the conservation of mass, momentum (during flow expansions), and energy head (during flow contractions) (STELLING and DUINMEIJER, 2003). This method, referred to as the *Flood Solver* within the Delft3D framework, was developed specifically to handle rapidly varying flows, accurately predict the rapid wetting and drying of grid cells, and be applicable to a wide range of Froude numbers (including subcritical and supercritical flows). This numerical method has been shown to model well a variety of dam break flooding problems (STELLING and DUINMEIJER, 2003), and the model formulation appears well suited for the simulation of long tsunami waves.

While the non-conservative form of the NLSWEs has no unique solution at local discontinuities, the use of conservative properties, as is done here, is often sufficient to provide solutions that are acceptable in terms of the local energy losses in and the propagation speed of a bore. This is because the conservation of mass and momentum should remain valid even for discontinuities in rapidly varying flows (i.e., breaking tsunami waves) (ZIJLEMA and STELLING, 2008), and because the dissipation of energy associated with wave-breaking-generated turbulence is inherently accounted for if momentum is conserved (HIBBERD and PEREGRINE, 1979; BROCCINI and PEREGRINE, 1996). However, the assumption of hydrostatic pressure (i.e., a basic assumption of the NLSWEs) is violated near the break point where vertical accelerations within the wave are necessary to balance the steepening of the wave front. Therefore, models based on the NLSWEs will not capture accurately the internal wave dynamics near the point of wave breaking. However, once breaking has started, wave front steepening is balanced by wave-breaking-generated turbulence (SVENDSEN and MADSEN, 1984), and the NLSWEs should be valid for predicting the run-up of broken waves (ZIJLEMA and STELLING, 2008).

A variety of methods are available to model the rapid wetting and drying of grid cells (i.e., the

moving shoreline) (see ZIJLEMA and STELLING, 2008 for a brief discussion of the methods available). Here a simple method that does not require special drying and flooding procedures is used (STELLING and DUINMEIJER, 2003), which ensures that the water depth is always positive and requires that only one grid cell is flooded or dried per time step. A single time step is chosen such that this criterion is met throughout each model simulation.

3. Numerical Experiments

The primary goal of this paper is to demonstrate the general applicability of the model for simulating tsunami inundation. The model is, therefore, compared with a wide array of different experiments that include several different types of initial wave forms, a wide range of initial nonlinearities, two- and three-dimensional basins, and breaking and non-breaking waves (Table 1). The input parameters used are not tuned to the observations, but instead physically realistic values were selected a priori. Owing to the limitations of using laboratory experiments and analytical solutions to evaluate tsunami inundation models and of using the NLSWEs to model solitary waves, the model-data comparisons focus on determining if the model is generally appropriate for simulating tsunamis (i.e., the model predictions are within $\sim 10\%$ of the observations for a variety of numerical and analytical benchmarks).

For the seven benchmark experiments, the model is run as a depth-averaged model. Friction is parameterized using Manning's formulation, with $n = 0.0001$ for the analytical solution where friction is neglected, and $n = 0.01$, a value consistent with smooth concrete (ARCEMENT and SCHNEIDER, 1990), for the six laboratory experiments. For each benchmark, an appropriate time step and grid cell size were selected to ensure all important wave and bathymetric features were resolved, the stability criterion in the model that prevents more than one grid cell from becoming wet/dry during a single time step was satisfied (i.e., $(\Delta t |u|)/\Delta x < 2$, where Δt is the time step, u is the flow velocity and Δx is the grid cell size), and the numerical experiments were simulated in an

efficient manner (i.e., the largest time step that resulted in no significant change in the results was used). Unless otherwise specified, the cross-shore location (x) is defined as positive onshore from the initial shoreline, the alongshore coordinate (y) is positive to the left of the centerline looking onshore, the elevation (h) is positive up from the still water level (SWL), and d is the water depth.

3.1. Run-up on a Planar Beach

3.1.1 Setup

The propagation of an initial free surface disturbance composed of a leading depression followed by a smaller amplitude crest (Fig. 1a, solid grey curve) over an idealized planar beach with a uniform slope of 1:10 (Fig. 1b, solid black line) was solved analytically using the initial-value-problem (IVP) technique (CARRIER *et al.*, 2003) and the solutions were provided by the organizers of the Third International Workshop on Long-Wave Run-up Models (LIU *et al.*, 2008). Cross-shore snapshots of the free surface elevation (Fig. 2a, solid black curves) and depth-averaged velocity (Fig. 2b, solid black curves) at $t = 160, 175$, and 220 s, representing the initial rundown, maximum rundown, and maximum run-up, respectively, were provided. Time series of the shoreline elevation (Fig. 2c, solid black curve) and velocity (Fig. 2d, solid black curve) from $t = 100$ to 280 s were also provided.

3.1.2 Results

Model predictions of the cross-shore water levels and depth-averaged velocities agree well with the analytical solution at all three time steps (Fig. 2a, b compare solid black and dashed grey curves). The predicted depth-averaged velocity increases sharply near the shoreline for $t = 160$ and 175 s, possibly owing to the depth dependence of the Manning friction formulation. However, this discrepancy is confined to water depths less than 0.2 m, and does not affect the model-data agreement in deeper water. The predicted shoreline elevation (Fig. 2c) and velocity (Fig. 2d) are in excellent agreement with the analytical solution.

Table 1
Benchmark summary

Benchmark	Benchmark type	Wave form	Initial wave height (m)	Offshore water depth (m)	Initial nonlinearity
(1) Planar beach	Analytical	Leading depression	~ 11	5,000	0.002
(2) Piece-wise linear beach	2-D laboratory	Solitary, impulse	0.06–0.54	0.51	0.12–1.06
(3) Alongshore non-uniform beach	3-D laboratory	Solitary	0.39	0.78	0.5
(4) Constant depth basin with conical island	3-D laboratory	Solitary	0.016, 0.032, 0.064	0.32	0.05, 0.10, 0.20
(5) Alongshore non-uniform beach with conical island	3-D laboratory	Solitary	0.39	0.78	0.5
(6) Complex 3-D bathymetry	3-D laboratory	Leading depression	~ 0.025	0.135	0.18
(7) Piece-wise linear beach with vertical wall	2-D laboratory	Solitary	0.011, 0.065, 0.153	0.218	0.05, 0.30, 0.70

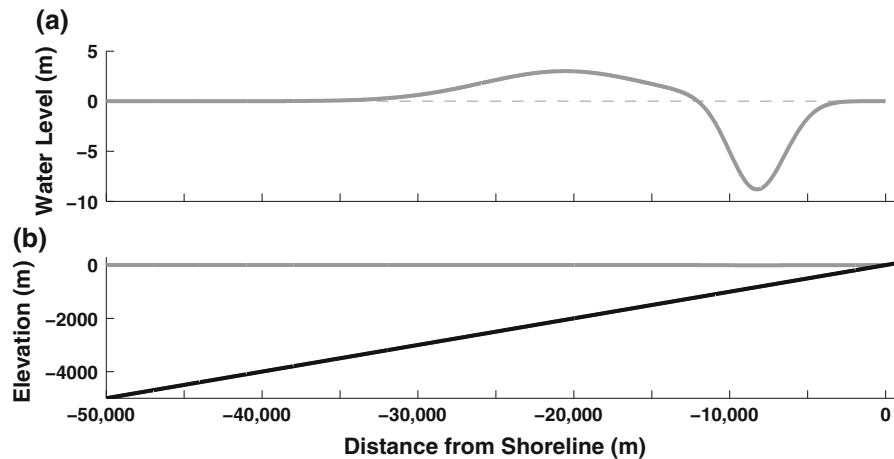


Figure 1

a Initial water level disturbance (solid grey curve) and still water level (dashed grey line) and **(b)** planar bathymetry with a slope of 1:10 (black curve) and initial water level (grey curve)

3.2. Run-up on a Piece-wise Planar Beach

3.2.1 Setup

A laboratory experiment using a two-dimensional piece-wise linear bathymetry was conducted in the large wave basin at Oregon State University (BALDOCK *et al.*, 2008) (Fig. 3). Ten different positive impulse or solitary waves (Table 2, Trial01–Trial10) were generated in 0.51 m water depth. The simulated waves range in nonlinearity ($\epsilon = H_i/d$, where H_i is the initial wave height) from 0.12 to 1.06, and include bores, shore breaks, and a non-breaking wave. Water levels were measured using 4 wire resistance wave gauges and 3 ultrasonic wave gauges. Flow velocities were measured using 5 Nortek acoustic doppler velocimeters (ADV). Two wire resistance wave

gauges and one ADV were located near the limit of the wave maker during all runs (e.g., Fig. 3, vertical hash labeled offshore) to ensure the repeatability and alongshore uniformity of the initial wave. The other wave gauges and ADVs were affixed to a movable bridge located at $x = -3.00, -1.50, -0.75, 0.00, 0.25, 0.50, 1.00, 2.00, 3.00$ and 6.00 m, respectively (Fig. 3, vertical hashes labeled bridge locations). All instruments were within ~ 0.5 m of the bridge location. Maximum inundation distances were recorded visually for all trials. The raw water level and velocity data were processed to remove spurious data (see BALDOCK *et al.*, 2008). However, as this data set has not been used extensively, the data were assessed visually, and time series containing significant noise or non-zero initial water levels were not

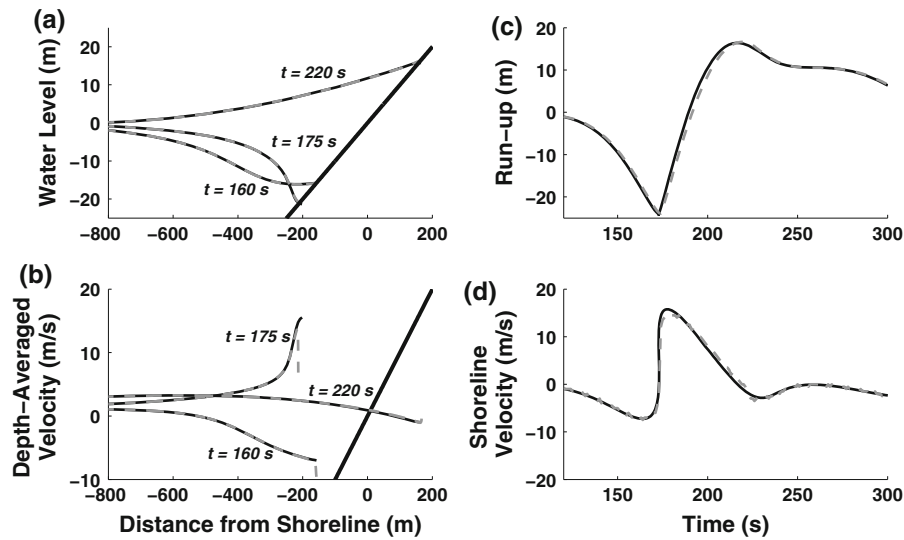


Figure 2

a Water levels and **(b)** depth-averaged velocities at $t = 160$, 175 , and 220 s and shoreline **(c)** elevation (i.e., run-up) and **(d)** velocity from the model predictions (*dashed grey curves*) and the analytical solution (*solid black curves*). The *thick black line* in **a** and **b** is the bed elevation

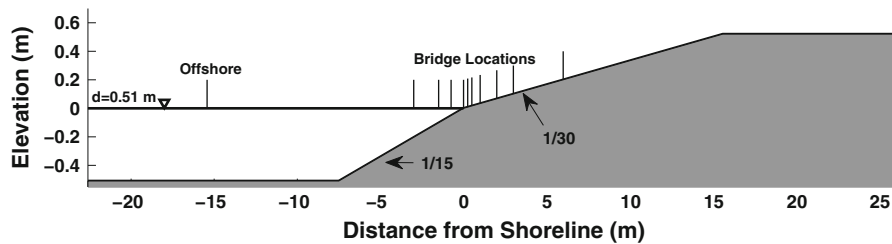


Figure 3

Model setup for the piece-wise planar beach. *Vertical hashes* indicate sensor or bridge locations

used. For further description of the model setup and initial analysis of the results see BALDOCK *et al.* (2008).

3.2.2 Results

The model predicts well (i.e., typically within 10%) the observed maximum inundation distance for 9 of the 10 trials (Fig. 4). The model predicts most accurately the inundation distance for waves with small initial nonlinearity, where dispersive effects are small. While the difference between the model predictions and observations generally increases with increasing inundation distance, the model does not appear to be biased toward over- or underpredicting the observations. The model significantly overpredicts the observed inundation distance for Trial01,

likely because the observed inundation distance, 15.6 m, occurs at the junction of the onshore slope and a horizontal section of the bathymetry (Fig. 3, $x = 15.6$ m). A small overestimation of the water velocity in shallow water will cause the wave to overtop this transition, and flow along the horizontal bed, resulting in a large change in the predicted inundation distance. For both the observations and model predictions the ratio of the maximum run-up elevation (R) to the initial wave height (H_i) is largest for the non-breaking wave, and decreases with increasing H_i (Table 2), suggesting that wave breaking reduces the inundation distance of a tsunami.

The model predicts well the observed wave height (within $\sim 10\%$) and wave arrival time (within 1 s) at most locations (e.g., Figs. 5 and 6), with the best model-data agreement found for the non-breaking

Table 2

Summary of initial wave conditions for the piece-wise linear beach. Table based on Table 3 in BALDOCK et al. (2008)

Trial #	Wave type	H_i (m)	Surf condition	Inundation distance (m)	R (m)	H_i/d	R/H_i
01	Impulse	0.55	Developed bore	15.6	0.52	1.06	0.95
02	Impulse	0.30	Bore	14.61	0.49	0.58	1.62
03	Impulse	0.17	Shore break	11.35	0.38	0.33	2.23
04	Impulse	0.13	Incipient breaker	10.46	0.35	0.25	2.68
05	Impulse	0.06	Non-breaking	5.97	0.20	0.12	3.32
06	Impulse	0.31	Shore break	11.48	0.38	0.60	1.23
07	Impulse	0.14	Shore break	8.34	0.28	0.27	1.99
08	Solitary	0.1	Incipient breaker	5.78	0.19	0.19	1.93
09	Solitary	0.25	Shore break	9.77	0.33	0.38	1.30
10	Solitary	0.35	Bore	11.83	0.39	0.67	1.13

wave (Fig. 5, Trial05), which has the smallest initial nonlinearity. As the model does not include dispersion, it does not reproduce accurately the wave shape at the offshore locations for highly nonlinear, dispersive waves (i.e., large ε). For these waves, the model predicts that the wave steepens and breaks further offshore than observed. However, the lack of dispersion in the model does not significantly affect the predicted timing of the initial wave, even when the wave has broken offshore of the measurement location (i.e., Fig. 5, Trial01 and Trial10).

The model predicts well the wave magnitude in shallow water and on land, and thus the total decrease in the wave height across the instrumented zone (Fig. 6d, Table 3). However, the model does not predict the observed shoaling near the break point

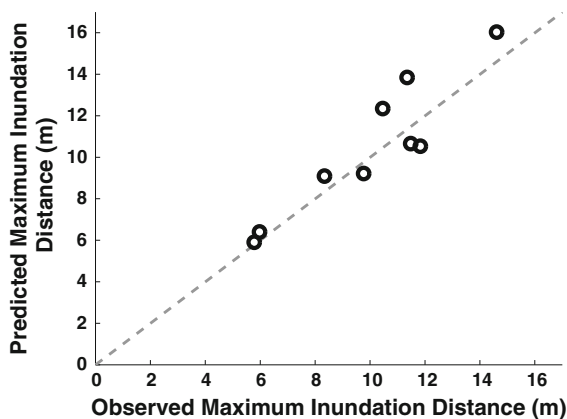


Figure 4

Maximum inundation distance from the observations and model predictions for Trial02–Trial10. Dashed grey line is perfect agreement

(e.g., Fig. 5, Trial10 and Fig. 6b) or the initial spike observed in the water levels during breaking (e.g., Fig. 5b, c, Trial10), though the model more accurately predicts the bore height that follows this spike. The good model-data agreement in terms of water levels for Trial01, which is highly nonlinear, at all bridge locations (e.g., Fig. 5, Trial01) is likely because all measurements were taken well onshore of the initial break point. The predicted dissipation in wave energy is owing to the shock-capturing numerical solution scheme used, and not bottom friction. For example, using very low values of n (i.e., a virtually frictionless model) does not affect the predicted decrease in wave height.

The model predictions compare well with the measured velocities for most trials and locations (e.g., Fig. 7). In shallow water the velocity is well predicted and increases rapidly as the wave front passes and then slowly decelerates until the flow is directed offshore (Fig. 7c, d). In deep water the velocity is less peaked and not as well predicted for highly nonlinear waves (Fig. 7a, b). Following run-down, differences occur in the observed and predicted time at which sensors become dry. However, this feature is highly sensitive to the value of n used.

3.3. Run-up on an Alongshore Non-Uniform Beach

3.3.1 Setup

An experimental setup designed to represent a steep, alongshore, non-uniform continental slope onshore of

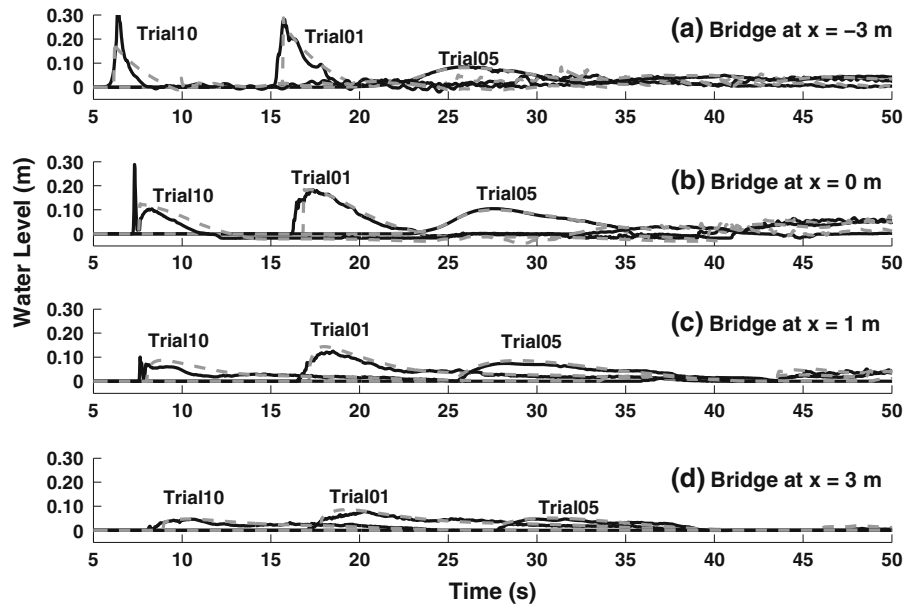


Figure 5

Water levels for Trial01, Trial05, and Trial10 measured using a resistance wave gauge (*solid black curves*) and predicted from the model (*dashed grey curves*) with the bridge located (a) -3 m, (b) 0 m, (c) 1 m, and (d) 3 m from the initial shoreline

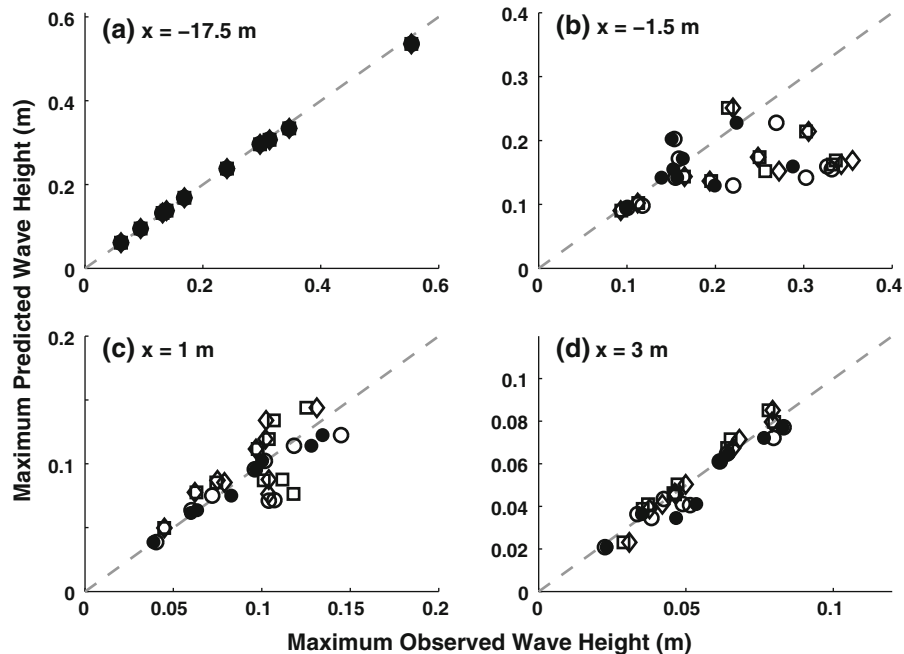


Figure 6

Maximum predicted and observed wave heights at four cross-shore locations for the resistance wire gauges (*squares and diamonds*) and sonic wave gauges (*open and filled circles*). *Dashed grey line* is perfect agreement, and positive x is shoreward of the initial shoreline

a deep, constant depth ocean was constructed in the large wave basin at Oregon State University (see SWILGER, 2009 for more details) (Fig. 8a). A solitary

wave 0.39 m high was generated in 0.78 m water depth and allowed to propagate shoreward. Owing to its large amplitude and high nonlinearity ($\epsilon = 0.5$),

Table 3

Initial wave heights (H_i) and the wave height at $x = 3$ m for the observations ($H_{3m,obs}$) and the model predictions ($H_{3m,pred}$) from the piece-wise linear beach

Trial	01	02	03	04	05	06	07	08	09	10
H_i (m)	0.55	0.30	0.17	0.13	0.06	0.31	0.14	0.10	0.25	0.35
$H_{3m,obs}$ (m)	0.078	0.08	0.065	0.064	0.047	0.046	0.037	0.029	0.035	0.046
$H_{3m,pred}$ (m)	0.085	0.08	0.072	0.067	0.05	0.046	0.041	0.023	0.039	0.046

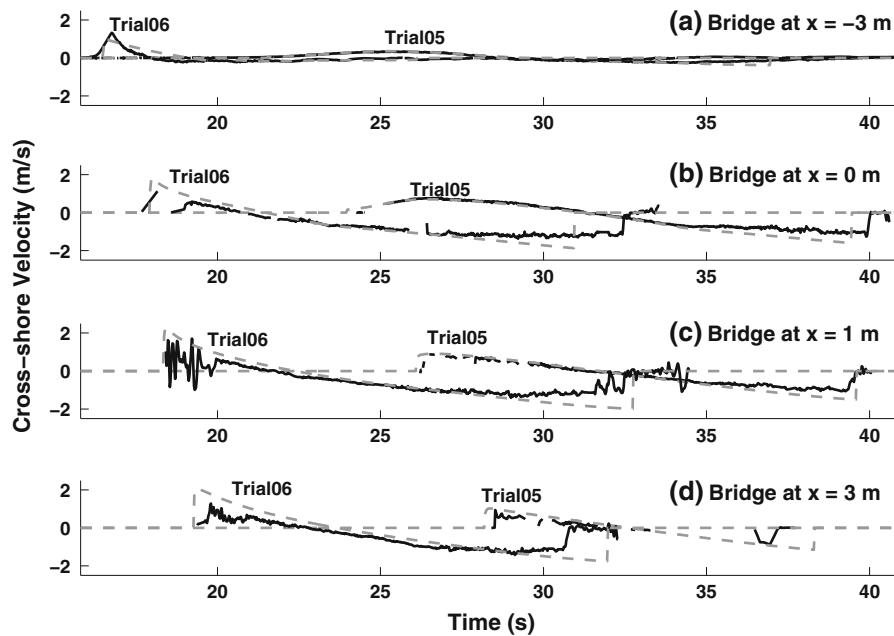


Figure 7

Cross-shore velocities during Trial05 and Trial06 from the observations (*solid black curves*) and model predictions (*dashed grey curves*) for the bridge located (a) -3 m, (b) 0 m, (c) 1 m, and (d) 3 m from the initial shoreline. The oscillations in the observed data occur because the sensors did not always obtain an accurate measurement, especially during the passage of a breaking wave

the solitary wave broke on the steep shelf slope. Water levels and velocities were measured at 17 and 3 locations within the basin, respectively (Fig. 8a, white circles). All observations were taken offshore of the initial shoreline, and no inundation data were provided. These observations were part of a larger experiment (see SWILGER, 2009), and the data used here were provided as part of the ISEC Community Workshop: Simulation and Large-Scale Testing of Nearshore Wave Dynamics (http://isec.nacse.org/workshop/isec_workshop_2009/).

3.3.2 Results

The model predicts well (i.e., within 10%) the magnitude and timing of the initial wave in the constant depth portion of the basin (Fig. 9a–b, compare solid and dashed curves). However, similar to what was observed for the piece-wise linear beach, the model does not accurately reproduce the observed wave shape at these locations. As the wave propagates over the steep shelf slope, it becomes more nonlinear and less dispersive, and the model predicts well the observed

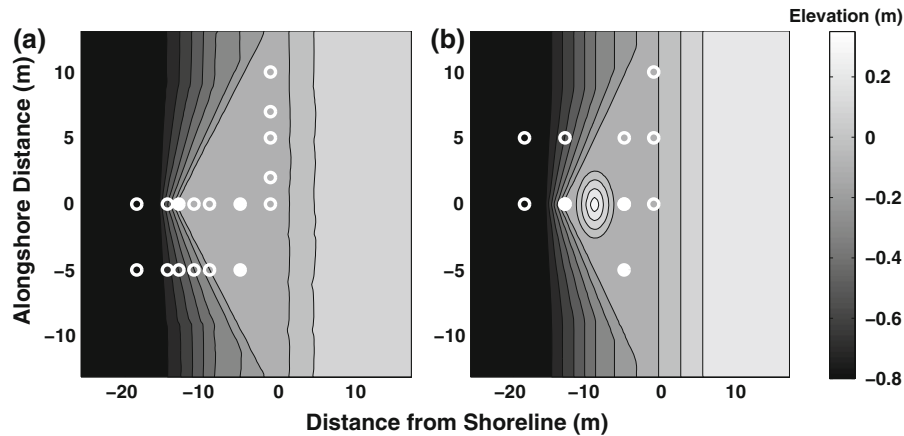


Figure 8

Model setup for (a) the alongshore non-uniform beach and (b) the alongshore non-uniform beach with a conical island. Open white circles are the locations where water level measurements are available, and solid white circles are where water level and velocity measurements are available. In b, only velocity was measured at $x = -5$ m, $y = -5$ m. Depth contours are in 0.10 m intervals from -0.80 to 0.40 m. The small differences observed in the depth contours between (a) and (b) are owing to the fact that the bathymetry provided in (a) is based on a lidar survey, while the bathymetry in (b) is based on the idealized experimental setup (i.e., no lidar was available)

timing, magnitude and shape of the initial wave (Fig. 9c–d). While the model predicts that the wave height decreases shoreward owing to breaking, at the most shoreward locations the maximum predicted wave heights are larger (by approximately 40%) and behind (by approximately 0.5 s) the observations (Fig. 9e–f). It is unclear why the model fails to predict the total decrease in wave height observed in this experiment given the good agreement found for the piece-wise linear beach. The discrepancies observed here may be owing to the steep slope of the beach and the proximity to wave breaking. Better model-data agreement might be expected further shoreward and on land where no observations were taken.

The model predicts well the large cross-shore velocities associated with the passage of the initial wave (e.g., Fig. 10a), but does not predict as accurately the smaller velocities associated with secondary and reflected waves. Away from the centerline, the model predicts the magnitude of the observed alongshore velocity, but the predictions lead the observations for the largest secondary wave (Fig. 10b, $t \sim 15$ – 20 s). This difference in the velocities is not related to bed friction (i.e., a larger n does not improve model-data comparisons), and may indicate the model overpredicts the wave speed in the very shallow water onshore of the instruments.

3.4. Run-up on a Circular Island

3.4.1 Setup

A conical island was constructed in the center of a constant depth basin at the US Army Corps of Engineers Waterways Experiment Station, Coastal Engineering Research Center (LIU *et al.*, 1995; BRIGGS *et al.*, 1995; KÁNOGLU and SYNOLAKIS, 1998) (Fig. 11). The island had a base diameter of 7.2 m with a slope of 1:4 rising to a height of 0.625 m (0.305 m above SWL). As the shoreline is circular, the cross-shore coordinate (x) is defined as positive onshore from the wave generating offshore boundary. Three solitary waves with $\varepsilon = 0.05, 0.1$, and 0.2 were generated in 0.32 m water depth and propagated through the basin. Water levels and run-up are compared at 4 (Fig. 11, white circles) and 9 locations, respectively. The values for the run-up were obtained from the benchmark website (<http://chl.erdc.usace.army.mil/>).

3.4.2 Results

Consistent with the experiment (LIU *et al.*, 1995), the model predicts the wave refracts around the island. The two refracted wave fronts collide in the lee of the island, driving flow up the back of the island (i.e., in

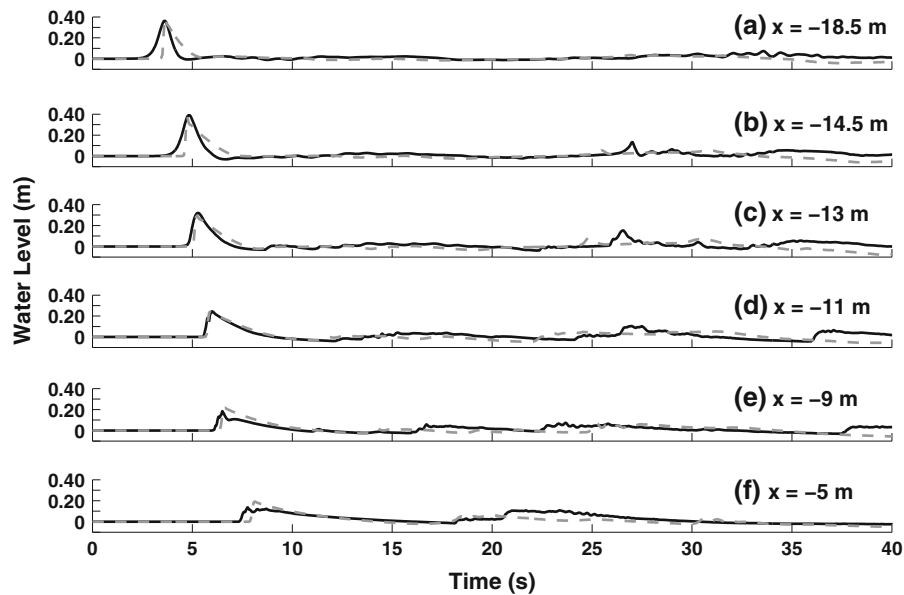


Figure 9

Water levels at 6 cross-shore locations along the centerline of the basin for the observations (*solid black curves*) and model predictions (*dashed grey curves*)

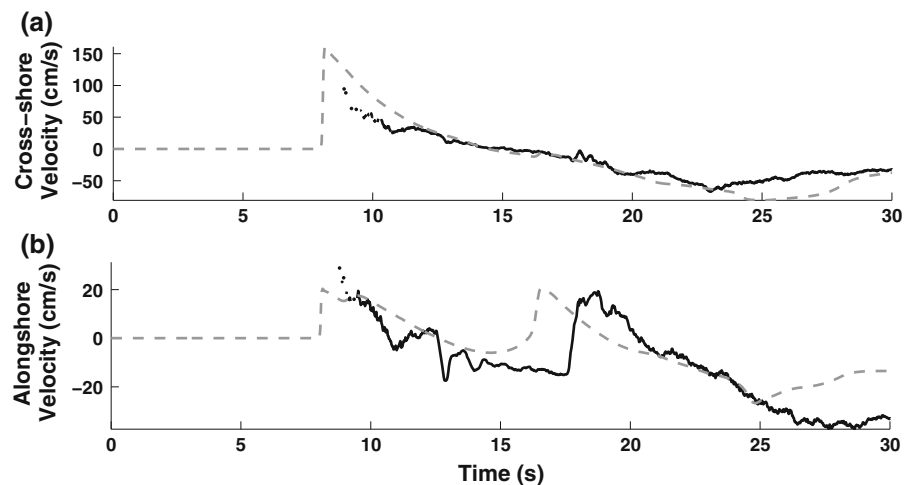


Figure 10

(a) Cross-shore and (b) alongshore velocities from the observations (*solid black curves*) and model predictions (*dashed grey curves*) for $x = -5$ m and $y = -5$ m

the direction opposite to initial wave propagation). The model predicts well the timing and magnitude of the observed water levels at the two locations in front of the island and the location to the side of the island (not shown). However, for large ε , the front of the predicted wave is steeper than the observations and

only for $\varepsilon = 0.05$ does the predicted wave shape match the observations. Behind the island, the model predicts well the timing of the observed increase in the water level owing to the arrival of the refracted waves, but underpredicts the magnitude by about 20, 30 and 50% for $\varepsilon = 0.05, 0.1,$ and $0.2,$ respectively.

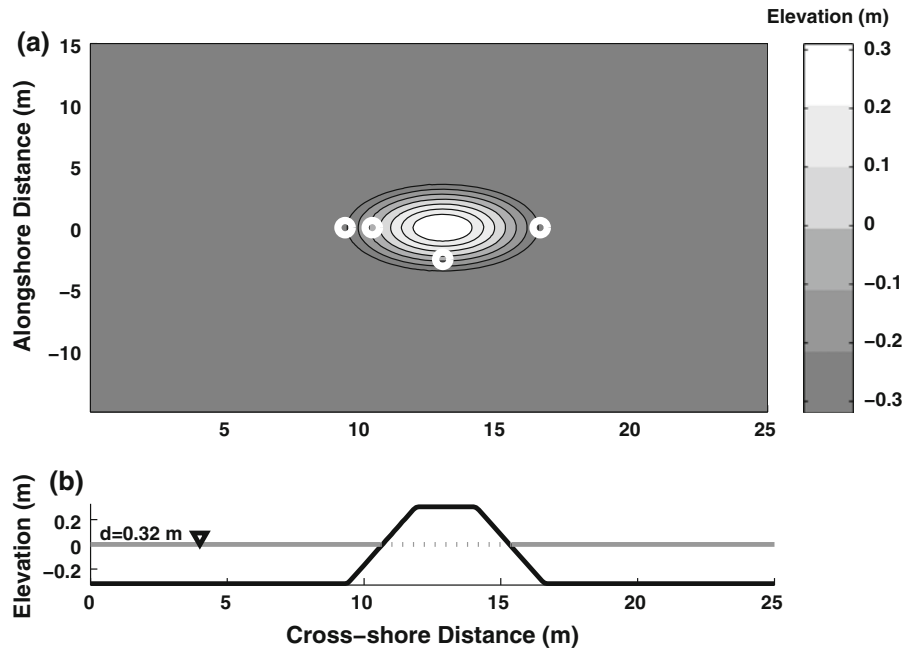


Figure 11
Model setup for the circular island amid a constant depth basin

The 50% underprediction for $\varepsilon = 0.2$ is similar to that found following TITOV and SYNOLAKIS (1997) (as shown in KÁNOGLU and SYNOLAKIS (1998)) but slightly larger than for the analytical solution presented by KÁNOGLU and SYNOLAKIS (1998).

The model predicts well the variation of run-up around the island for all three waves (Fig. 12). The model tends to overpredict the observations for small ε (Fig. 12a) and underpredict the observations for large ε (Fig. 12c). The former may be owing to the predicted oversteepening of the wave in shallow water due to the lack of dispersion in the model, while the latter is likely caused by the predicted waves breaking offshore of the island.

3.5. Run-up on an Alongshore Non-Uniform Beach with a Conical Island

3.5.1 Setup

The underlying bathymetry in this experiment is identical to that described in Sect. 3.3.1 for the alongshore non-uniform beach, except that a conical island was added at the apex of the steep shelf slope (Fig. 8b). A solitary wave 0.39 m high was generated

in 0.78 m water depth and breaks on the steep shelf slope. Water levels and velocities were measured at 9 and 3 locations, respectively (Fig. 8b, white circles). Owing to the formation of a strong wake immediately behind the island, the sensor located here did not accurately record the water level or flow velocity (Pat Lynett, pers. comm.), and these measurements are not used. These data were provided as part of the ISEC Community Workshop: Simulation and Large-Scale Testing of Nearshore Wave Dynamics (http://isec.nacse.org/workshop/isec_workshop_2009).

3.5.2 Results

The results for the measured water levels and velocities are similar to those presented in Sect. 3.3.2, and are not discussed here. Instead comparisons are made with two features created by the addition of the island. These include the formation of a wake in the lee of the island following the passage of the initial wave (Fig. 13, top panels) and the convergence of four secondary waves slightly behind and to the side of the island (Fig. 13, bottom panels). Owing to the limited observational data available at these locations, the model results are

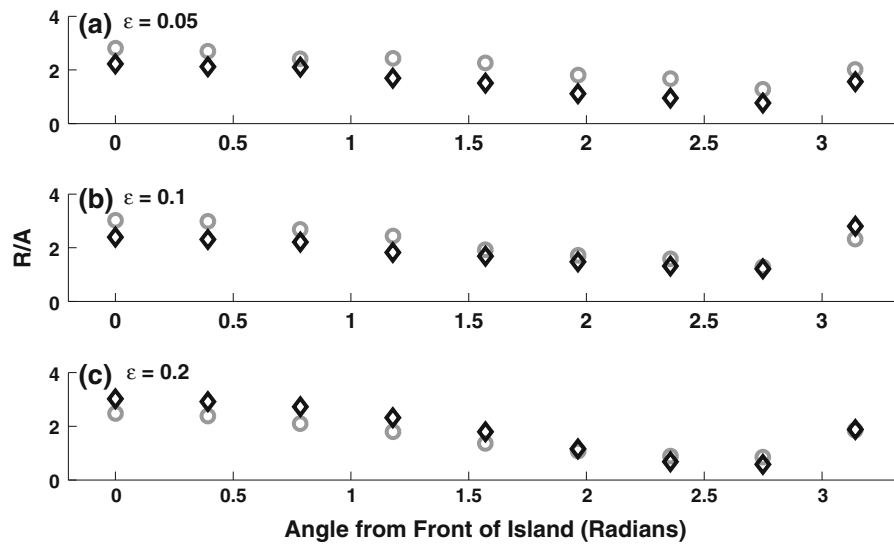


Figure 12

Normalized run-up (R/A), where A is the wave amplitude, for the observations (*black diamonds*) and model predictions (*grey circles*) for $\epsilon =$ (a) 0.05, (b) 0.1, and (c) 0.2

compared qualitatively with snapshots taken from video recordings of the experiments (Pat Lynett, pers comm.).

The model predicts the formation of a wake behind the island, but the shape differs somewhat from the observations (Fig. 13, compare top right and left panels). Similarly, the model predicts the convergence of four secondary waves, but the magnitude, timing, and location of each wave differs somewhat from the observations (Fig. 13, compare bottom right and left panels). The slight misalignments of the four waves likely account for the failure of the model to capture the signal of this convergence in the water level and the velocity time series (not shown) at the single observation location (Fig. 13, black circle in the bottom left panel).

3.6. Run-up on a Complex 3-D Beach

3.6.1 Setup

A 1:400 scale laboratory experiment of the impact of the 1993 Okushiri tsunami on Monai, Okushiri Island, Japan, including realistic bathymetry and topography scaled to the tank, was conducted in The Central Research Institute for Electric Power Industry (CRIEPI) in Abiko, Japan (Liu *et al.*, 2008) (Fig. 14a). The experiment was forced with a leading

depression N-wave at the offshore model boundary in 0.135 m water depth (Fig. 14b). Water level data were provided at 3 stations inshore of the offshore island (Fig. 14a). Owing to the complex shoreline, the cross-shore coordinate (x) for this experiment is positive shoreward from the wave generating offshore boundary, and the alongshore coordinate (y) is positive from the right side of the experimental basin facing onshore.

3.6.2 Results

The model predictions are in excellent agreement with the observations at all three stations for the initial wave (Fig. 15). The wave crest arrives at approximately $t = 15$ s, with the model predictions lagging the observations by less than 1 s and the wave magnitude predicted within 10%. After the first wave, the observed water levels are highly influenced by reflections off the topography and closed boundaries. The model predicts the arrival of the first reflected wave at approximately $t = 35$ s, but the predictions both lead and are larger than the observations. While the model predicts the arrival of a series of secondary waves at all three locations, the accuracy of the predictions of these reflected waves decreases with increasing time (Fig. 15, $t > 55$ s).

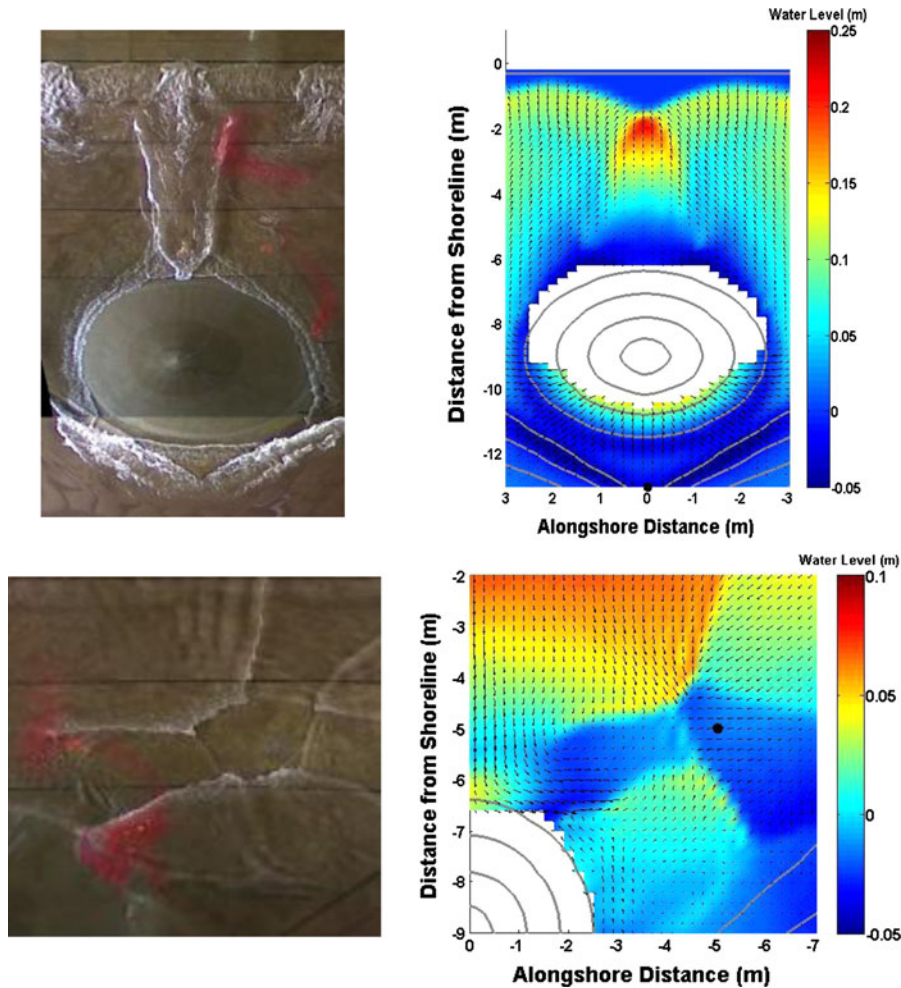


Figure 13

Snapshots of the water surface just after the passage of the initial wave (*top left panel*) and just as four secondary waves are about to collide (*bottom left panel*) and the predicted water levels (*color contours*) and velocities (*vectors*) for similar times (*right panels*). The *black circles* and the *solid curves* in the *right panels* are the location of an ADV and the depth contours, respectively. Note these panels are rotated 90° counterclockwise with regards to Fig. 8b

3.7. Run-up on a Vertical Wall

3.7.1 Setup

A piece-wise linear bathymetry composed of slopes of 1:53, 1:150, and 1:13 and ending in a vertical wall was constructed in a 23.2 m long, 0.45 m wide flume (BRIGGS *et al.*, 1996) (Fig. 16). Three solitary waves with $\varepsilon = 0.05$, 0.3, and 0.7 were generated in 0.218 m water depth. Water levels are compared at 6 locations (Fig. 16). The maximum run-up was recorded as the highest point water reached on the vertical wall. For $\varepsilon = 0.3$ and 0.7, the waves broke

near the wall and between gauges 7 and 8, respectively. The wave did not break for $\varepsilon = 0.05$.

3.7.2 Results

For $\varepsilon = 0.05$ (case A), the model predicts well the timing, magnitude, and shape of the incoming wave (e.g., Fig. 17a–c). The timing and magnitude of the reflected wave are well predicted by the model, but the predicted wave has a steeper vertical face than observed (Fig. 17a, b). This discrepancy in the reflected wave shape is because the predicted wave

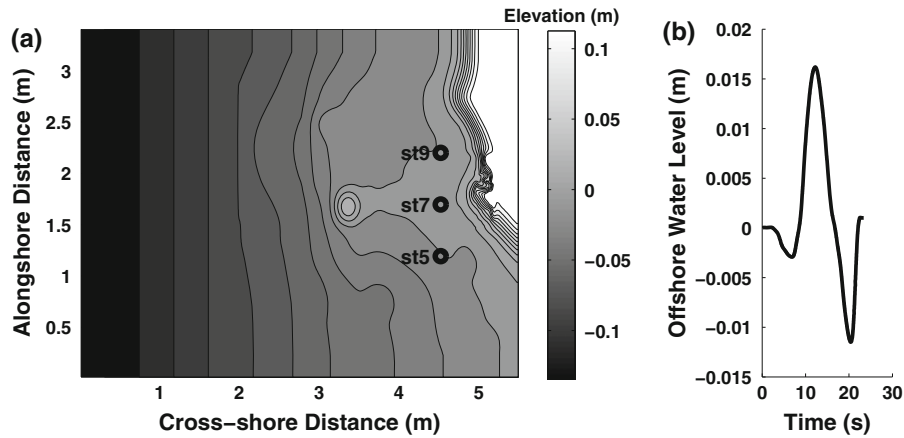


Figure 14

a Model setup and (b) water level at the offshore boundary for the complex 3-D beach. The location of the three water level stations are labeled st5, st7, and st9 in (a)

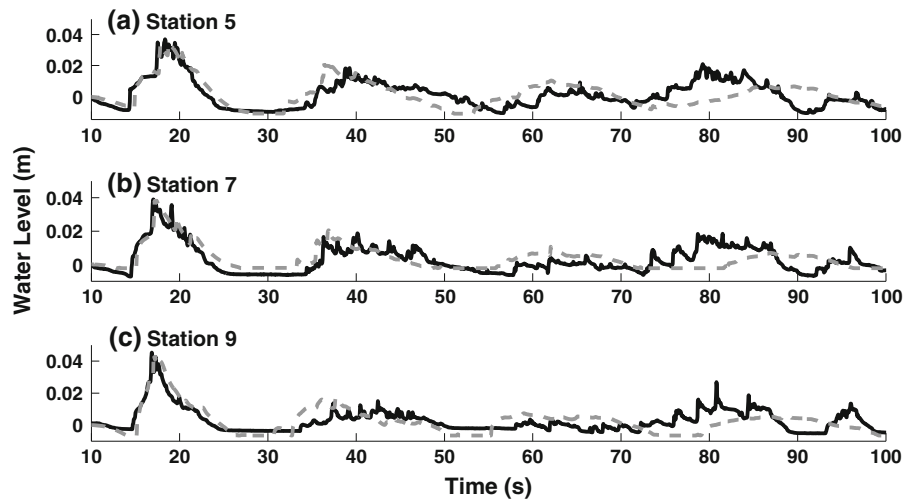


Figure 15

Water levels at the three stations for the observation (*solid black curves*) and the model predictions (*dashed grey curves*)

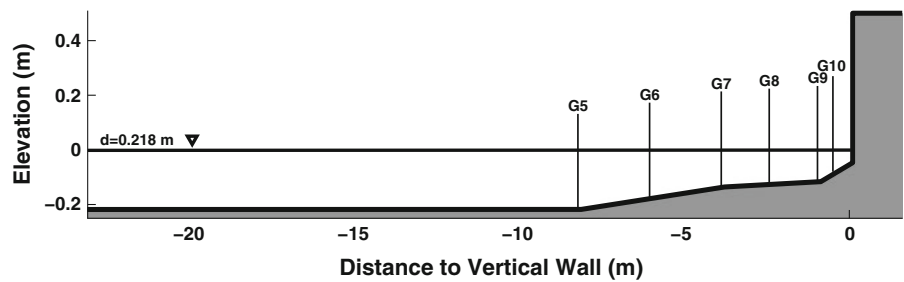


Figure 16

Model setup for the piece-wise linear beach ending in a vertical wall

steepens in the shallow water before reaching the wall, and maintains this steepened shape after reflecting seaward. Conversely, the inherent dispersion of the solitary wave keeps the observed wave from steepening both before and after reflection. The predicted maximum run-up of 0.0246 m is within approximately 10% of the observed maximum of 0.0274 m.

For $\varepsilon = 0.3$ and 0.7 (cases B and C, respectively), dispersion becomes more important, and the model predicts well the timing, amplitude, and shape of the incoming wave only at station 5 (Fig. 17d, g). Further shoreward the model predicts that the wave steepens and breaks at a location more offshore than observed. Significant differences exist between the modeled and observed reflected waves in terms of both the wave magnitude and shape, likely owing to the way a broken or breaking wave interacts with a vertical surface. While the timing of the reflected wave is generally well predicted for $\varepsilon = 0.3$, for $\varepsilon = 0.7$ the predictions lead the observations by about 1 s at the most seaward location (Fig. 17g). The predicted maximum run-up values of 0.0936 m and 0.154 m for $\varepsilon = 0.3$ and 0.7 , respectively, are about 4 and 2 times smaller than the observed values of 0.4572 m and 0.2743 m. This underprediction is likely owing to the measured run-up being a result of wave-breaking-

generated spray, which the model cannot predict, as well as other local breaking processes that are not included in the model. Differences in the wave shape as it reaches the wall owing to a lack of dispersion in the model may also contribute to the observed underprediction.

3.8. Kuala Meurisi, Sumatra

3.8.1 Setup

Bathymetry, topography, and maximum water level estimates were collected following the 26 December 2004 Indian Ocean tsunami near Kuala Meurisi on the north coast of Sumatra, Indonesia (JAFJE *et al.*, 2006; GELFENBAUM *et al.*, 2007) (Fig. 18a). The maximum water levels were mostly estimated from broken branches, and may represent minimum values of the actual water levels. The bathymetry was measured along seven cross-shore transects, while topography was measured only along a single transect. As the bathymetry is approximately alongshore uniform, a one-dimensional, depth-averaged model with a cross-shore grid spacing of 12 m is used. The offshore water level variation was obtained from the output of a deep water ocean propagation model and an estimate of the initial source disturbance for the 26

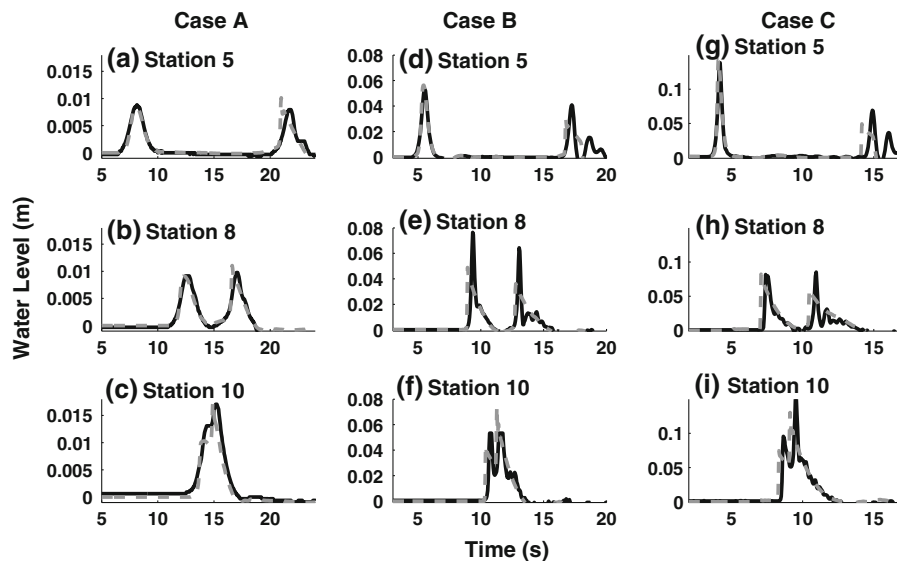


Figure 17

Water levels for $\varepsilon =$ (a–c) 0.05, (d–f) 0.3, and (g–i) 0.7 at station (a, d, g) 5, (b, e, h) 8, and (c, f, i) 10 for the model (solid black curves) and observations (dashed grey curves). In each panel, the first and second waves are the incident and reflected waves, respectively

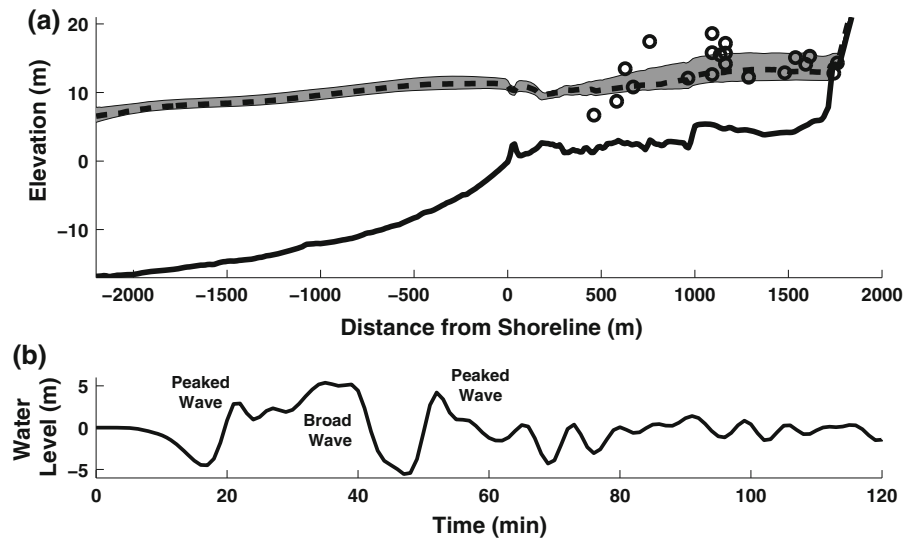


Figure 18

a Observed (black circles) and predicted (dashed black curve) maximum water levels at Kuala Meurisi. The solid black curve is the combined bathymetry and topography and the shaded grey area represents the range of maximum water levels predicted for the three simulations conducted. **b** Offshore wave level shoaled to 17 m water depth

December 2004 tsunami (VATVANI *et al.*, 2005a, b) (Fig. 18b). Due to the coarse resolution of the deep water model, the offshore water level variation was available only in 35 m water depth. As the high resolution nearshore bathymetry used in this study extends only to 17 m water depth (Fig. 18a), Green's law ($H \sim h^{1/4}$) is used to shoal the predicted waves from 35 to 17 m water depth. This shoaling produces approximately a 20% increase in the wave height of the water level variation used to force the model simulation. Changes in the wave length are inherently included by forcing the model with a time series, given that the wave period remains relatively constant. However, no attempt was made to simulate the change in wave shape due to shoaling. The entire wave train, which is composed of three large waves (i.e., two peaked waves and a broad wave) followed by a series of smaller waves, is simulated. This wave forcing is a simplification of the actual tsunami as it is assumed to be normally incident, and therefore neglects waves propagating at angles to the coast, such as trapped and scattered waves, and may not capture accurately all wave reflections off nearby land masses. Bed roughness is estimated using Manning's formulation with $n = 0.025$ and 0.032 off- and

onshore. A larger onshore roughness is used to take into account the presence of vegetation.

3.8.2 Results

The model predicts the run-up elevation well, but overpredicts the observed water levels closest to the shoreline while underpredicting the water levels further shoreward (Fig. 18a, compare dashed black curve and open circles). The observed overprediction near the shoreline may be owing to biased estimates of the observed water levels, as no large trees remained standing after the tsunami. Given the large uncertainty in the model setup, including in the offshore water level and bed roughness, the assumption of alongshore uniformity, the use of bathymetry taken after the tsunami, and the exclusion of local obstacles such as houses and trees, the model predicts the observations surprisingly well.

As a first step to quantify the effect of the uncertainty on the maximum water level predictions, two further simulations were conducted. The first was forced using the unshoaled water level variation predicted in 35 m water depth (i.e., an assumed lower bound on the wave forcing). The second was forced using a 40% increase in the water level from 35 m

water depth coupled with a 50% decrease in the on- and offshore roughness (i.e., an assumed upper bound). These simulations indicate that while the uncertainty has an effect on the predictions, the predictions from all three simulations fall within the range of the observations (Fig. 18a, compare shaded grey area and black circles). Future work will examine in more detail the sensitivity of the flow predictions to the input conditions.

4. Discussion

4.1. Solitary Waves as Tsunamis

Over the past few decades many analytical and laboratory studies of tsunami propagation and inundation have used solitary waves as proxies for tsunami waves. It was first suggested by HAMMACK (1973), SEGUR (1973), and HAMMACK and SEGUR (1974, 1978a, b) that a positive initial surface disturbance of arbitrary shape (i.e., an initial tsunami wave generated in deep water) will eventually devolve into a series of solitary waves if the propagation distance is long enough. Based on this observation and the fact that solitary waves are easily reproducible in the laboratory, are defined by only two parameters (i.e., H_i and d), and can be modeled in the limited spatial scales of most laboratory facilities, solitary waves have continued to be used extensively to model tsunamis, including in 5 of the 7 benchmarks examined in this study.

Recently, however, a growing number of authors have questioned the relevance of solitary waves as proxies for tsunamis (MADSEN *et al.*, 2008; CONSTANTIN and JOHNSON, 2008; CONSTANTIN, 2009). Using geophysically realistic scales of nonlinearity and dispersion, these studies demonstrate that the distance necessary for earthquake-generated tsunami waves to devolve into solitons can be several times the fetch of the largest ocean basin. Further limiting the relevance of solitary waves as proxies for tsunamis is the fact that their nonlinearity and length are not independent. Instead, the relative length of a solitary wave decreases with increasing nonlinearity. Owing to the limited spatial dimensions of most laboratory facilities and the need to record measurable

hydrodynamics, usually only highly nonlinear, and thus relatively short, solitary waves are simulated. For example, in the laboratory studies examined here, the nonlinearity of the solitary waves varies from 0.05 to 0.67. However, the nonlinearity of actual tsunamis observed away from the nearshore is typically much smaller than this, and previous studies (MADSEN *et al.*, 2008) have suggested that solitary waves with $\varepsilon > 0.05$ are not long waves, and are more similar to wind waves than to tsunamis.

Furthermore, observations and eyewitness accounts from several recent tsunamis indicate that the largest wave does not always arrive first (e.g., PAPADOPOULOS *et al.*, 2006; CHOOWONG *et al.*, 2008) and that the first wave can arrive as a leading depression (TADEPALLI and SYNOLAKIS, 1996). Both of these observations argue against the development of solitons, which requires the largest wave to arrive first and be of positive orientation. Some studies have suggested that leading depression N-waves are a better representation of tsunamis (TADEPALLI and SYNOLAKIS, 1994, 1996). However, these waves are difficult to generate in the laboratory and have not been widely used in experimental studies. Furthermore, the use of single waves, whether of solitary or N shape, will not produce wave–wave interactions, which may be important for accurately predicting both the maximum inundation distance and sediment transport of tsunamis.

Unfortunately, the limited horizontal dimensions of laboratory facilities and the difficulty of generating more complex wave forms will limit the nonlinearity, number, and shape of the waves that can be generated. Therefore, until more realistic experiments can be conducted or more detailed observations from actual tsunamis recorded, these laboratory experiments will remain an important aspect of validating tsunami propagation and inundation models.

4.2. Scaling Up to Sediment Transport

Extending numerical models to include sediment transport increases the complexity and uncertainty of the model. For example, near bed fluid velocities and the suspension of sediment are highly sensitive to the bed roughness, which may vary significantly

spatially. Calculating sediment transport also requires the delineation of the sediment source characteristics (i.e., location, grain-size distribution, thickness), which are often poorly constrained, as well as the use of transport formulations developed empirically for lower velocity flows.

Unfortunately, no standardized benchmarks currently exist with which to verify model predictions of tsunami-induced sediment transport, though preliminary work conducted as part of a workshop held in Friday Harbor, Washington, in 2007 has shown some initial success (HUNTINGTON *et al.*, 2007). The development of laboratory-scale benchmarks is not straightforward because these benchmarks must include and balance the effects of sediment suspension, advection, and settling on the appropriate time and length scales. This is difficult given the limited size of most laboratory facilities and the fact that sediment becomes cohesive at small grain sizes. The use of solitary waves, which dominate laboratory studies, may not be appropriate because the flow velocities and accelerations induced are likely to be different than those induced by long tsunami waves. Development of sediment transport benchmarks based on field observations of sediment deposits collected after a tsunami is hindered by the fact that the initial conditions (i.e., the nearshore wave form, sediment source characteristics) and onshore roughness, especially in the presence of vegetation, are typically poorly constrained. Furthermore, even good agreement with observed water levels (i.e., Sect. 3.8.2), often the only hydrodynamic information available, does not necessarily imply good agreement with the time-varying velocities, which dictate the suspension and transport of sediment, that occurred during the inundating tsunami.

The difficulties associated with modeling tsunami-induced sediment transport notwithstanding, the Kuala Meurisi simulation conducted in Sect. 3.8 was extended to include the suspension and transport of sediment. First, the water column was subdivided into ten vertical sigma layers (i.e., layers representing a constant percentage of the water column), with increasing resolution near the bed, to accurately represent the bottom boundary layer. An erodable sediment bed 5 m thick, with a mean grain size of 400 μm was assumed to exist over the entire model

domain. While the erodable bed thickness at this site is unknown, the maximum predicted scour is less than 5 m, and therefore the onshore deposition of sediment is not limited by the thickness used. Sediment transport is calculated by solving the conservation of mass equations within the hydrodynamic model. Bedload and suspended load transport are calculated following VAN RIJN (1993; 2007a, b) combined with a $k\text{-}\epsilon$ turbulence model. Bedload is calculated based on a sediment mobility number and the critical velocity for the initiation of motion. Suspended load is calculated based on a near-bed reference concentration and a vertical diffusion coefficient determined from the output of the turbulence model. Sediment fluxes between the water column and the bed are calculated within each grid cell based on the vertical diffusion of sediment owing to turbulent mixing and deposition from settling, and the bottom morphology is updated accordingly at each time step (LESSER *et al.*, 2004; VAN RIJN *et al.*, 2004). Sediment-induced density stratification owing to high suspended sediment concentrations is inherently accounted for within the turbulence model by adjusting the fluid density to include the mass of the suspended sediment. The settling velocity is determined based on the clear water settling velocity of VAN RIJN (1993) combined with the effects of hindered settling following RICHARDSON and ZAKI (1954). The combined sediment transport/morphological change model has been shown to model well many coastal and estuarine settings (LESSER *et al.*, 2004; GERRITSEN *et al.*, 2007; VAN RIJN *et al.*, 2007).

Using this simplified setup, the model predicts the observed sediment deposit thickness generally within a factor of 2, though locally the predictions can be off by more than an order of magnitude (Fig. 19, compare dashed grey curve with black circles). Both model simulations and field measurements show thicker deposits in local topographic lows and thinner deposits or erosion on local topographic highs. Most of the sediment is deposited by the second peaked wave, although a smaller fraction is deposited by the first peaked wave. Very little sediment was eroded or deposited by the broad wave. The observed peak in sediment thickness near the cliff is composed of fine sediment and is not captured by the model which uses only a single grain size. Given the high level of

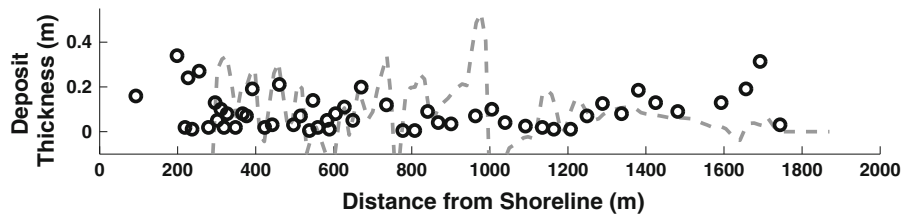


Figure 19

Deposit thickness measured near Kuala Meurisi (*black circles*) and change in bed elevation predicted by the model (*dashed grey curve*)

uncertainty involved in the model setup, the model-data agreement is remarkably good. More work needs to be done to examine the details of the predicted sediment transport and deposition to ensure that the model is accurately capturing the appropriate processes. However, the detailed analyses required are beyond the scope of this paper, and will be the subject of future work.

4.3. Model Applicability

Delft3D predicts well the general hydrodynamic observations associated with tsunami nearshore propagation and inundation measured under a wide range of conditions. This study, combined with previous studies (VATVANI *et al.*, 2005a, b; GELFENBAUM *et al.*, 2007) that showed Delft3D models well the deep-water propagation and inundation of the 26 December 2004 Indian Ocean tsunami near Banda Aceh, demonstrates that Delft3D is applicable for modeling long, non-dispersive tsunamis from the source to the maximum extent of inundation.

As Delft3D is based on the NLSWEs, which are derived using the assumption of hydrostatic pressure, the model does not include dispersive terms and is best suited to tsunamis where the wavelength is long compared to the water depth. The model-data comparisons presented here support this, with the model predicting most accurately the observations from benchmarks where the wave is long (*i.e.*, the analytical solution over a planar beach) and where dispersion is relatively less important (*i.e.*, Trial05 from the piece-wise linear experiment). Therefore, Delft3D is likely appropriate for modeling most earthquake-induced tsunamis, which normally have very long wavelengths and experience negligible frequency dispersion over typical propagation distances.

As stated previously, comparisons with laboratory observations offer only qualified validation of model applicability. Therefore, while the model predictions are in reasonable agreement with benchmarks in which dispersion is important (*i.e.*, highly nonlinear solitary waves), this does not necessarily imply the model is appropriate for modeling highly dispersive tsunamis. Tsunamis generated by landslides, volcanic eruptions, and meteoroid impacts can have wavelengths of the same order of magnitude as the water depth, and frequency dispersion can be important even near the source. A previous study (LYNETT *et al.*, 2003) found large differences between offshore wave height predictions from models based on the NLSWEs and on the Boussinesq equations, which allow for weak frequency dispersion, for the landslide-generated component of the 1998 Papua New Guinea tsunami. Therefore it is unclear how accurately Delft3D will model the deep-water propagation of highly dispersive waves such as those generated by a landslide.

The good model-data agreement demonstrates the numerical solution method employed is appropriate for modeling the general characteristics (*i.e.*, wave height, run-up, velocities) of both breaking and non-breaking waves. The advantage of this numerical solution technique over many Boussinesq models is that it does not require a breaking criterion, but inherently captures the loss of energy associated with wave breaking. Furthermore, the accuracy of the predictions onshore of breaking does not appear to decrease for waves with higher initial nonlinearity (*e.g.*, Fig. 5d), which may suggest depth-limited breaking masks the effects of frequency dispersion onshore of breaking. A previous study (LYNETT *et al.*, 2003) found similar nearshore wave height predictions using both an NLSWE and a Boussinesq model for the landslide-generated component of the 1998

Papua New Guinea tsunami even though the model predictions further offshore were significantly different. It was suggested that the similarity in the nearshore wave height predictions was owing to depth-limited breaking. While this may imply that Delft3D can be used to model the run-up and inundation of breaking, dispersive waves, under exactly what conditions the NLSWEs accurately represent the hydrodynamics of dispersive tsunamis onshore of breaking remains to be determined.

While the model predicts well the overall dissipation of wave energy owing to breaking, the model does not predict local breaking dynamics such as the generation of turbulence or vertical flow accelerations. Even for waves that are non-dispersive in deep water, dispersion becomes important close to breaking where it balances the increasing nonlinearity associated with shoaling and delays breaking (CONSTANTIN and JOHNSON, 2008). As the model does not include dispersion, it will predict that waves break further offshore than physically realistic. Therefore, while the model may predict well the water levels and velocities before and after breaking, as well as the maximum run-up elevations of breaking waves, it is not appropriate for simulating wave characteristics near the breakpoint. Furthermore, the model may underpredict the run-up and inundation of waves close to breaking, as the lack of dispersion will cause these otherwise non-breaking waves to break and dissipate energy.

The generally good agreement with the observed water levels and flow velocities suggests extension of the model to include sediment transport may be appropriate for long, non-breaking waves generated by earthquakes. However, extension of the model may not be appropriate for dispersive or breaking waves. In the case of dispersive waves, the wave shape, and thus the cross-shore distribution of velocity, is poorly predicted, and the model may misrepresent the distribution of the bed stress. For breaking waves, the location and magnitude of wave-breaking-generated turbulence, which the model does not predict for long waves, will affect the patterns of sediment suspension, transport, and deposition.

5. Conclusions

The model predicts well the hydrodynamic observations (i.e., water levels, velocities, and inundation distances) from seven analytical and laboratory experiments and the maximum water levels observed near Kuala Meurisi, Sumatra, following the 26 December 2004 tsunami. Model predictions agree best with experiments where dispersion is less important. The model predicts well the total decrease in wave height and the speed of breaking waves. However, the model does not reproduce the observed shoaling for some waves or the shape of highly nonlinear waves in deep water. These results indicate the model is appropriate for simulating tsunami propagation and inundation for both breaking and non-breaking long waves (i.e., most earthquake-induced tsunamis) but may not be appropriate for modeling highly dispersive tsunamis, such as those generated by landslides or impacts, especially over long distances.

Extension of the model to include sediment transport is shown to produce reasonable results for long, non-breaking waves, but may not be appropriate in the case of breaking or dispersive waves. While including sediment transport increases the complexity of and uncertainty in the model, the model predicts the sediment deposition at Kuala Meurisi generally within a factor of two. These results suggest that the coupling of validated tsunami-induced sediment transport models with paleo-tsunami deposits could aid in the improvement of local tsunami hazards assessments.

Acknowledgements

This research was funded by a USGS Mendenhall Post-Doctoral Fellowship and the USGS Coastal and Marine Geology Program. Reviews provided by Eric Geist, Pat Lynett, Utku Kânoğlu, and 2 anonymous reviewers greatly improved this manuscript. Edwin Elias is thanked for his help and guidance concerning the details of the numerical model.

REFERENCES

- ARCAS, D. and AITOV, V. (2006), *Sumatra tsunami: lessons from modeling*, *Surv. Geophys.*, 27, 679-705.
- ARCEMENT, G. and SCHNEIDER, V. (1990), *Guide for selecting Manning's roughness coefficients for natural channels and flood plains*, Water Supply Pap., U.S. Geol. Surv., Reston, VA.
- ATWATER, B.F. (1987), *Evidence for great Holocene earthquakes along the outer coast of Washington State*, *Science*, 236, 942-944.
- BALDOCK, T.E., COX, D., MADDUX, T., KILLIAN, J., and FAYLER, L. (2008), *Kinematics of breaking tsunami wave fronts: A dataset from large scale laboratory experiments*, *Coastal Eng.*, doi: 10.1016/j.coastaleng.2008.10.011.
- BRIGGS, M.J., SYNOLAKIS, C.E., HARKINS, G.S., and GREEN, D.R. (1995), *Laboratory experiments of tsunami run-up on a circular island*, *Pure Appl. Geophys.*, 144, 569-593.
- BRIGGS, M.J., SYNOLAKIS, C.E., KANOGLU, U., and GREEN, D.R. (1996), *Benchmark Problem #3: Runup of solitary waves on a vertical wall*, "Long-wave Runup Models," International Workshop on Long Wave Modeling of Tsunami Runup, Friday Harbor, San Juan Island, WA, September 12-16, 1995.
- BROCCHINI, M. and PEREGRINE, D. (1996), *Integral flow properties of the swash zone and averaging*, *J. Fluid Mech.*, 317, 241-273.
- CARRIER, G.F. and GREENSPAN, H.P. (1958), *Water waves of finite amplitude on a sloping beach*, *J. Fluid Mech.*, 4, 97-109.
- CARRIER, G.F., WU, T.T., and YEH, H. (2003), *Tsunami run-up and draw-down on a plane beach*, *J. Fluid Mech.*, 475, 79-99.
- CHOOWONG, M., MURAKOSHI, N., HISADA, K., CHARUSIRI, P., CHAROENTITIRAT, T., CHUTAKOSITKANON, V., JANKAEW, K., KANJANAPAYONT, P., and PHANTUWONGRAJ, S. (2008), *2004 Indian Ocean tsunami inflow and outflow at Phuket, Thailand*, *Mar. Geol.*, 248, 179-192.
- CONSTANTIN, A. (2009), *On the relevance of soliton theory to tsunami modeling*, *Wave Motion*, 6, 420-426.
- CONSTANTIN, A. and JOHNSON, R.S. (2008), *Propagation of very long waves, with vorticity, over variable depth, with applications to tsunamis*, *Fluid Dyn. Res.*, 40, 175-211.
- FRITZ, H., BORRERO, J., SYNOLAKIS, C., and YOO, J. (2006), *2004 Indian Ocean flow velocity measurements from survivor videos*, *Geophys. Res. Lett.*, 33, L24605.
- GELFENBAUM, G., VATVANI, D., JAFFE, B., and DEKKER, F. (2007), *Tsunami inundation and sediment transport in the vicinity of coastal mangrove forest*, Conference Proceedings Coastal Sediment '07, doi: 10.1061/40926(239)86.
- GERRITSEN, H., DE GOEDE, E.D., PLATZEK, F.W., GENSEBERGER, M., VAN KESTER, J.A.Th.M., and UITTENBOGAARD, R.E. (2007), *Validation document for Delft3D-Flow*, Rep. X0356, Delft Hydraulics, Delft, The Netherlands.
- GONZALEZ, F., BERNARD, E., MEINIG, C., EBLE, M., MOFJELD, H., and STALIN, S. (2005), *The NTHMP Tsunami network*, *Nat. Hazards*, 35, 25-29.
- GONZÁLEZ, F.I., GEIST, E.L., JAFFE, B., KANOGLU, U., MOFJELD, H., SYNOLAKIS, C.E., TITOV, V.V., ARCAS, D., BELLOMO, D., CARLTON, D., HORNING, T., JOHNSON, J., NEWMAN, J., PARSONS, T., PETERS, R., PETERSON, C., PRIEST, G., VENTURATO, A., WEBER, J., WONG, F., and YALCINER, A., (2009), *Tsunami pilot study working group "Probabilistic tsunami hazard assessment at Seaside, Oregon for near- and far-field seismic sources,"* *J. Geophys. Res.*, 114, C11023, doi:10.1029/2008JC005132.
- HAMMACK, J. (1973), *A note on tsunamis: Their generation and propagation in an ocean of uniform depth*, *J. Fluid Mech.*, 60(4), 769-799.
- HAMMACK, J. and SEGUR, H. (1974), *The Korteweg-deVries equation and water waves, part 2: Comparison with experiments*, *J. Fluid Mech.*, 65(2), 289-314.
- HAMMACK, J. and SEGUR, H. (1978a), *The Korteweg-deVries equation and water waves, part 3: Oscillatory waves*, *J. Fluid Mech.*, 84(2), 337-358.
- HAMMACK, J. and SEGUR, H. (1978b), *Modeling criteria for long waves*, *J. Fluid Mech.*, 84(2), 359-373.
- HIBBERD, S. and PEREGRINE, D. (1979), *Surf and run-up on a beach: a uniform bore*, *J. Fluid Mech.*, 95, 323-345.
- HUNTINGTON, K., BOURGEOIS, J., GELFENBAUM, G., LYNETT, P., JAFFE, B., YEH, H., and WEISS, R. (2007), *Sandy signs of a tsunami's onshore depth and speed*, *EOS Trans.*, 88(52), 577-584.
- JAFFE, B. and GELFENBAUM, G. (2007), *A simple model for calculating tsunami flow speed from tsunami deposits*, *Sediment. Geol.*, 200, 347-361.
- JAFFE, B., BORRERO, J., PRASETYA, G., PETERS, R., McADOO, B., GELFENBAUM, G., MORTON, R., RUGGIERO, P., HIGMAN, B., DENGLER, L., HIDAYAT, R., KINGSLEY, E., KONGKO, W., LUKIJANTO, MOORE, A., TITOV, V., and YULIANTO, E. (2006), *Northwest Sumatra and offshore islands field survey after the December 2004 Indian Ocean tsunami*, *Earthquake Spectra*, 22, 105-135.
- KANOGLU, U. (2004), *Nonlinear evolution and runup-rundown of long waves over a sloping beach*, *J. Fluid Mech.*, 513, 363-372.
- KANOGLU, U. and SYNOLAKIS, C.E. (1998), *Long wave runup on piecewise linear topographies*, *J. Fluid Mech.*, 374, 1-28.
- LIU, P.L.-F., CHO, Y.S., BRIGGS, M.J., KANOGLU, U., and SYNOLAKIS, C.E. (1995), *Run-up of solitary waves on a circular island*, *J. Fluid Mech.*, 302, 259-285.
- LIU, P.L.-F., YEH, H., and SYNOLAKIS, C.E. (ed.) (2008), *Advanced numerical models for simulating tsunami waves and run-up*, *Advances in Coastal and Ocean Engineering*, 10.
- LESSER, G.R., ROELVINK, J.A., VAN KESTER, J.A.T.M., and STELLING, G.S. (2004), *Development and validation of a three-dimensional morphological model*, *Coastal Eng.*, 51, 883-915.
- LYNETT, P., BORRERO, J., LIU, P., and SYNOLAKIS, C.E. (2003), *Field survey and numerical simulations: A review of the 1998 Papua New Guinea Tsunami*, *Pure Appl. Geophys.*, 160, 2119-2146.
- MADSEN, P., FUHRMAN, D., and SCHAFER, H. (2008), *On the solitary wave paradigm for tsunamis*, *J. Geophys. Res.*, 113, C12012, doi: 10.1029/2008JC004932.
- NANAYAMA, F., FURUKAWA, R., SHIGENO, K., MAKINO, A., SOEDA, Y., and IGARASHI, Y. (2007), *Nine unusually large tsunami deposits from the past 4000 years at Kiritappu marsh along the southern Kuril Trench*, *Sediment. Geol.*, 200, 275-294.
- PAPADOPOULOS, G., CAPUTO, R., McADOO, B., PAVLIDES, S., KARATATHIS, V., FOKAEFS, A., ORFANOIANNAKI, K., and VALKANIOITIS, S. (2006), *The large tsunami of 26 December 2004: Field observations and eyewitness accounts from Sri Lanka, Maldives Is. and Thailand*, *Earth, Planets, Space*, 58, 233-241.
- RICHARDSON, J.F. and ZAKI, W.N. (1954), *Sedimentation and fluidization: Part I*, *Trans. Inst. Chem. Eng.*, 32, 35-50.
- SEGUR, H. (1973), *The Korteweg-deVries equation and water waves, part 1: Solutions of the equations*, *J. Fluid Mech.*, 59(4), 721-735.
- SMITH, D.E., FOSTER, I.D.L., LONG, D., and SHI, S. (2007), *Reconstructing the pattern and depth of flow onshore in a paleo-*

- tsunami from associated deposits*, *Sediment. Geol.*, *200*, 362-371.
- STELLING, G.S. and DUINMEIJER, S.P.A. (2003), *A numerical method for every Froude number in shallow water flows, including large scale inundations*, *Int. J. Num. Meth. in Fluids*, *43*, 1329-1354.
- STELLING, G.S. and LEENDERTSE, J.J. (1991), *Approximation of convective processes by cyclic ACI methods*. In: *Proceedings of 2nd ASCE Conference on Estuarine and Coastal Modeling*, Tampa, USA, 771-782.
- STELLING, G.S. and VAN KESTER, J.A.T.M. (1994), *On the approximation of horizontal gradients in sigma coordinates for bathymetry with steep bottom slopes*, *Int. J. Num. Meth. in Fluids*, *18*, 915-935.
- SVENDSEN, I.A. and MADSEN, P.A. (1984), *A turbulent bore on a beach*, *J. Fluid Mech.*, *148*, 73-96.
- SWILGER, D.T. (2009), *Laboratory study investigating the three dimensional turbulence and kinematic properties associated with a breaking solitary wave*, Master Thesis, Texas A&M.
- SYNOLAKIS, C.E. (1987), *The run-up of solitary waves*, *J. Fluid Mech.*, *185*, 523-545.
- SYNOLAKIS, C.E., BERNARD, E.N., TITOV, V.V., KANOGLU, U., and GONZALEZ, F. (2007), *Standards, criteria, and procedures for NOAA evaluation of tsunami numerical models*, NOAA OAR Special Report, Contribution No 3053, NOAA/OAR/PMEL, Seattle, Washington.
- SYNOLAKIS, C.E., BERNARD, E.N., TITOV, V.V., KANOGLU, U., and GONZALEZ, F. (2008), *Validation and verification of tsunami numerical models*, *Pure Appl. Geophys.*, *165*, 2197-2228.
- TADEPALLI, S. and SYNOLAKIS, C.E. (1994), *The run-up of N-waves on sloping beaches*, *Proc. R. Soc. Lond.*, *445*, 99-112.
- TADEPALLI, S. and SYNOLAKIS, C.E. (1996), *Model for the leading waves of tsunamis*, *Phys. Rev. Lett.*, 2141-2144.
- TANG, L., TITOV, V., and CHAMBERLIN, C. (2009), *Development, testing, and application of site-specific tsunami inundation models for real-time forecasting*, *J. Geophys. Res.*, *114*, C12025, doi:10.1029/2009JC005476.
- TITOV, V. and SYNOLAKIS, C.E. (1997) *Numerical modeling of 2-D and 3-D long wave runup using VTSC-2 and VTSC-3*. In *Long wave runup models* (ed. H. Yeh et al.), World Scientific, 242-248.
- TITOV, V., GONZALEZ, F., BERNARD, E., EBLE, M., MOFJELD, H., NEWMAN, J., and VENTURATO, A., (2005), *Real-time tsunami forecasting*, *Natural Hazards*, *35*(1), 45-58.
- U.S. Agency for International Development (USAID) (2005), Fact sheet, July 7. http://www.usaid.gov/our_work/humanitarian_assistance/disaster_assistance/countries/Indian_ocean/fy2005/indianocean_et_fs39-07-07-2005.pdf.
- VAN RIJN, L.C. (1993), *Principles of sediment transport in rivers, estuaries and coastal seas*, Aqua Publications, Amsterdam.
- VAN RIJN, L.C. (2007a), *Unified view of sediment transport by currents and waves. I: Initiation of motion, bed roughness, and bed-load transport*, *J. Hydraul. Eng.*, *133*, 649-667.
- VAN RIJN, L.C. (2007b), *Unified view of sediment transport by currents and waves. II: Suspended transport*, *J. Hydraul. Eng.*, *133*, 668-689.
- VAN RIJN, L.C., WALSTRA, D.J.R., and VAN ORMONDT, M. (2004), *Description of TRANSPOR 2004 (TR2004) and implementation in DELFT3D-online*, Rep. Z3748, Delft Hydraulics, Delft, The Netherlands.
- VAN RIJN, L.C., WALSTRA, D., and VAN ORMONDT, M. (2007), *Unified view of sediment transport by currents and waves. IV: Application of morphodynamic model*, *J. Hydraul. Eng.*, *133*, 776-793.
- VATVANI, D., SCHRAMA, E., and VAN KESTER, J. (2005a), *Hindcast of tsunami flooding in Aceh-Sumatra*, Proc. of the 5th International Symposium on Ocean Wave Measurement and Analysis, Madrid, Spain.
- VATVANI, D., BOON, J., and RAMANAMURTY, P.V. (2005b), *Flood risk due to tsunami and tropical cyclones and the effect of tsunami excitations on tsunami propagations*, Proc. of the IAEA Workshop on External Flooding Hazards, Tamil Nadu, India.
- WEI, Y., BERNARD, E., TANG, L., WEISS, R., TITOV, V., MOORE, C., SPILLANE, M., HOPKINS, M., and KANOGLU, U. (2008), *Real-time experimental forecast of the Peruvian tsunami of August 2007 for U.S. coastlines*, *Geophys. Res. Letters*, *35*, L04609.
- YEH, H., LIU, P., and SYNOLAKIS, C.E., (ed.) (1996), *Proc. Int. Symposium*, Friday Harbor, USA, 12-17 September 1995, *Long-Wave Rump Models*, World Sci., Singapore.
- ZULEMA, M. and STELLING, G.S. (2008), *Efficient computation of surf zone waves using the nonlinear shallow water equations with non-hydrostatic pressure*, *Coastal Eng.*, *55*, 780-790.

(Received January 21, 2010, revised December 8, 2010, accepted December 19, 2010, Published online March 4, 2011)